Short communication

# Improved cycling behavior of ZEBRA battery operated at intermediate temperature of 175 °C

Guosheng Li, Xiaochuan Lu, Jin Y. Kim*, John P. Lemmon, Vincent L. Sprenkle

*Pacific Northwest National Laboratory, Richland, WA 99352, USA*

## HIGHLIGHTS

- A Pt grid was applied to the BASE surface to overcome the low wettability of sodium melt on the BASE at 175 °C.
- These Pt-modified cells provided deeper charging than the cells with standard BASEs, and cell cycling performances were stable.
- This improved performance is attributed to the better distribution of sodium melt on the BASEs and expanded active area.

## ARTICLE INFO

## ABSTRACT

Operation of the sodium–nickel chloride battery at temperatures below 200 °C reduces cell degradation and improves cyclability. One of the main technical issues with operating this battery at intermediate temperatures such as 175 °C is the poor wettability of molten sodium on $\beta''$-alumina solid electrolyte (BASE), which causes reduced active area and limits charging. In order to overcome the poor wettability of molten sodium on BASE at 175 °C, a Pt grid was applied on the anode side of the BASE using a screen printing technique. Cells with their active area increased by metallized BASEs exhibited deeper charging and stable cycling behavior.

Published by Elsevier B.V.

## 1. Introduction

Among ZEBRA-type batteries, a sodium–nickel chloride (Na–NiCl$_2$) redox pair has been investigated for decades as a promising electric energy storage device for renewable energy and smart grid applications [1,2]. The overall electrochemical reaction of a Na–NiCl$_2$ battery can be described as [3]:

$$2Na + NiCl_2 \leftrightarrow 2NaCl + Ni, \quad E_0 = 2.58\ V \qquad (1)$$
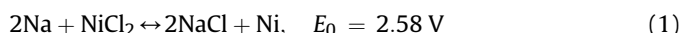
The conventional tubular Na–NiCl$_2$ battery is typically operated at relatively high temperatures around 300 °C in order to improve the ionic conductivity of the $\beta''$-alumina solid electrolyte (BASE) and the secondary liquid electrolyte as well as the wettability of molten sodium on the BASE [3–5]. The secondary electrolytes used for ZEBRA-type batteries are corrosive at these temperatures, requiring special sealing technologies such as thermal compression

bonding [3]. Furthermore, it was reported that the degradation of cell performance is accelerated at high operating temperatures due to the rapid growth of NaCl and Ni particles [6]. Recently, a new planar Na–NiCl$_2$ battery containing a new low-melting-temperature catholyte (NaBr–NaCl–AlCl$_3$) was developed by us that had stable cycling performance at intermediate temperatures (below 200 °C) [7].

In order to achieve adequate, stable electrochemical performance at intermediate temperatures, the interfacial polarization between molten sodium and $\beta''$-alumina (BASE) must be kept as low as possible. In other words, the molten sodium has to be in good contact with the full active area of the $\beta''$-alumina surface throughout the cycling process [8]. Various treatments of the BASE surface, including a lead treatment, have been reported to improve the wettability of molten sodium on the BASE [9,10]. However, the wettability of molten sodium is still insufficient at the intermediate temperatures, causing incomplete coverage of molten sodium on the BASE and thereby limiting the charging [6].

In this work, metallization on the anode side of the BASE was attempted by applying a Pt grid on the BASE in order to expand

* Corresponding author. Tel.: +1 509 375 2225; fax: +1 509 375 2186.
  *E-mail addresses:* Jin.Kim@pnnl.gov, jinykim8z@gmail.com (J.Y. Kim).

triple-phase boundaries and achieve full utilization of the active area. The effects of platinum metallization combined with lead treatment on charging capacity and cycling behaviors at the intermediate temperature of 175 °C will be discussed.

## 2. Experimental

The detailed cell configurations and cell preparation procedures have been described in our previous publications [6,7]. Briefly, homemade composite BASE disks (500 μm thick) consisting of yttria-stabilized zirconia and β″-alumina solid electrolyte (BASE) were glass-sealed to an α-alumina fixture to separate cathode and anode chambers [7,11]. The cathode granules comprising Ni, NaCl, and additives were put into the cathode chamber, and then the secondary electrolyte ($NaAlCl_4$) was vacuum-infiltrated into the granules. For the typical button cells with 3 $cm^2$ active area, the weight of cathode granules (molar ratio of Ni to NaCl = 1.82) was 1 g, corresponding to a theoretical capacity of 157 mAh.

Two different methods of surface modification were attempted on the anode sides of the BASEs: (1) A standard BASE was prepared with lead treatment in which a saturated lead acetate aqueous solution was applied on the anode surface of the BASE, followed by a heat treatment at 400 °C in nitrogen. (2) A metallized BASE was prepared by applying a platinum grid with 75% coverage on the anode side of the BASE, using a conventional screen printing technique. After screen printing, the BASE was sintered at 900 °C in air (Pt grid thickness: ~5 μm after sintering). Similar to standard BASEs, the metallized BASE was also treated with lead acetate.
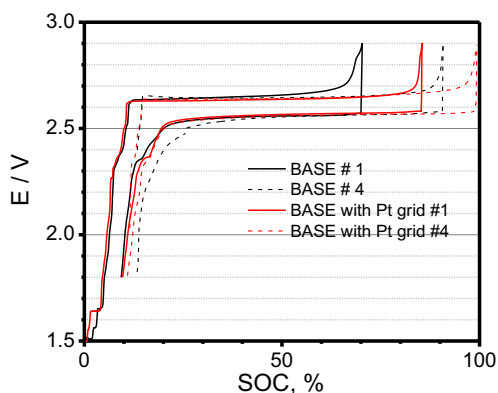
The assembled button cells were then placed in a furnace and heated to 175 °C. The cell tests were performed using an Arbin potentiostat, adopting two different cell testing schedules. Initially, full maiden charge/discharge cycling was applied between cutoff voltages of 1.8 V (for discharging) and 2.9 V (for charging) at a constant current of 10 mA in order to obtain maximum charge capacity. After four full cycles, a standard cycling process was started with a fixed capacity window between 40 and 130 mAh (27−87% state of charge, SOC). The charge process of standard cycling consists of a two-step charging process. During the first step, the cells were charged up to a capacity of 80 mAh at a current of 30 mA (fast charging, C/3 with respect to the cycling capacity of 90 mAh). During the second step, the remaining capacity (10 mAh) was charged at 10 mA (slow charging, C/9) to achieve the full charging capacity. The discharge process was a single-step discharging with a constant current of 30 mA (C/3). Cutoff voltages of

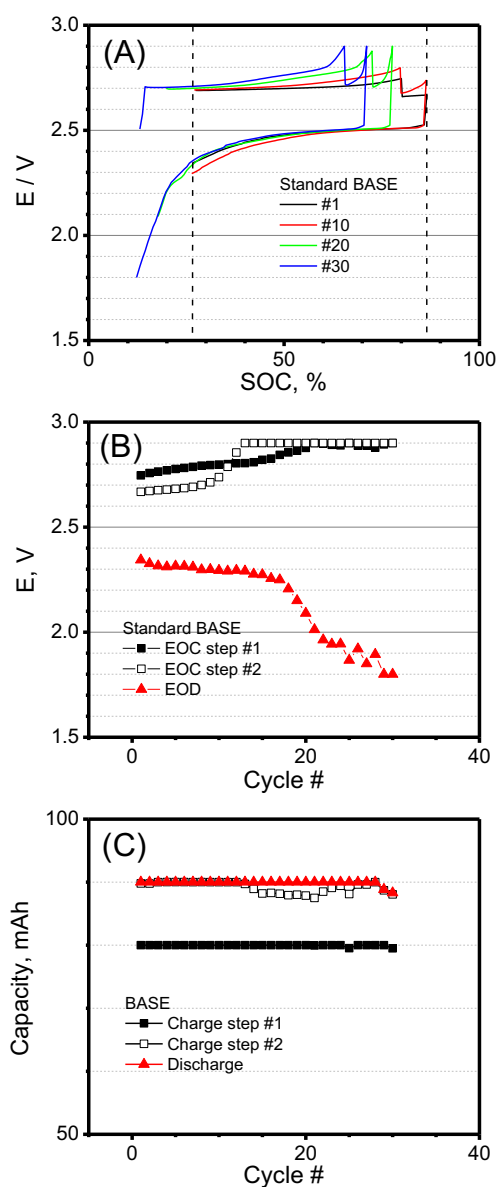2.9 V and 1.8 V were applied to avoid overcharge and overdischarge, respectively.

## 3. Results and discussion

The voltage profiles (E vs. SOC) of full maiden charge/discharge cycling are shown in Fig. 1. For the first charge, the cell with a metallized BASE reached 85% SOC at the end of charge while the one with a standard BASE charged up to only 70% SOC. The charging capacity increased with cycles, reaching 99% SOC for the metallized BASE and 90% SOC for the standard BASE at the end of the fourth charge. The significantly deeper charging observed on the metallized BASE indicates the better coverage of molten sodium on the BASE.

The performance of the cell with a standard BASE under a standard fixed-capacity cycling process at the higher current of C/3 is shown in Fig. 2. As can be seen in voltage profiles (Fig. 2A), the

**Fig. 2.** Cycling performance of the cell with a standard BASE tested under standard fixed-capacity cycling (90 mAh). (A) Voltage profiles vs. SOC, (B) EOC and EOD voltages vs. cycles, and (C) capacity vs. cycles.

**Fig. 1.** Voltage profiles of maiden charge/discharge cycling between the cutoff voltages of 2.9 V and 1.8 V. The first and fourth full cycles are shown to compare the extent of charging for the cells containing a standard BASE (black) and a metallized BASE with a Pt grid (red). (For interpretation of the references to color in this figure legend, the reader is referred to the web version of this article.)

charging capacity decreased with cycles at a fast current of C/3, possibly due to the insufficient wetting of molten sodium. The end-of-charge (EOC) voltage also rapidly increased with cycles and reached the cutoff voltage of 2.9 V within 10 cycles (Fig. 2B). Capacity vs. cycle plots (Fig. 2C) revealed limited charging capacity from the tenth cycle since the voltage reached the cutoff voltage of 2.9 V, leading to a shift of the cycling window down to a more discharged state under fixed-capacity cycling. With this shift to a more discharged state, the end-of-discharge (EOD) voltage also decreased and reached the discharge cutoff voltage of 1.8 V as shown in Fig. 2B. These results clearly indicate a fast degradation of the cell with a standard BASE due to limitation in charging capacity at the higher current.

In contrast to the fast degradation observed on the cell with a standard BASE, a cell containing a metallized BASE showed stable performance (Fig. 3). The voltage profiles collected during standard fixed-capacity cycling overlapped quite well as cycles increased, as

shown in Fig. 3A. The EOC voltages (Fig. 3B) were also fairly stable with cycles below the cutoff voltage of 2.9 V, resulting in full charging capacity. Since the full capacity can be charged, no shift in the cycling window was observed (Fig. 3A), and the EOD voltage was stable around 2.3 V (Fig. 3B), leading to no capacity degradation (Fig. 3C).

These different cell performances can be attributed to the sodium anode since both cells have identical cathode materials, and cell configurations are identical except for the Pt grid. Schematics shown in Fig. 4 represent the differences in active area made by the application of the Pt grid on the anode side of the BASE. In the case of cells with standard BASEs (Fig. 4A), the sodium melt tends to have a localized distribution due to its high viscosity and poor wettability on the BASE at 175 °C. Therefore, the active area is localized only on the area of the BASE in contact with the sodium melt. The localized active area of the BASE causes an inefficient utilization of the cathode materials and hence limited charging, since the electrochemical reaction of cathode materials excluded from the active area creates a large polarization and overpotential. This is in good agreement with the experimental observation of the maiden charge/discharge process, in which cells with the standard BASEs achieved a limited charging capacity (70% SOC). On the other hand, the cells with metallized BASEs sustained extended charging and achieved higher capacity. Since the Pt grid provides an electrical path over the entire anode side of the BASE, molten sodium can be generated during charging on a larger area as shown in Fig. 4B. Even though the wettability of molten sodium on the BASE is not improved, the utilization of the cathode materials on the metallized BASE can increase compared to that of the standard BASE due to the better distribution of the sodium melt on the anode side. This is consistent with the experimental results, in which deeper charging was observed on the cells with the metallized BASEs (85% SOC for the first charge and 99% SOC for the fourth charge) compared to the standard BASE (70% SOC for the first charge and 90% SOC for the fourth charge). When cells were cycled at a higher current of C/3, the sodium in the cells with standard BASEs became more localized with cycles, resulting in the fast cell degradation and decreased charging capacity observed in Fig. 2B. The stable cycling performance for the cells with the metallized BASEs indicates that the Pt grid helps maintain the better
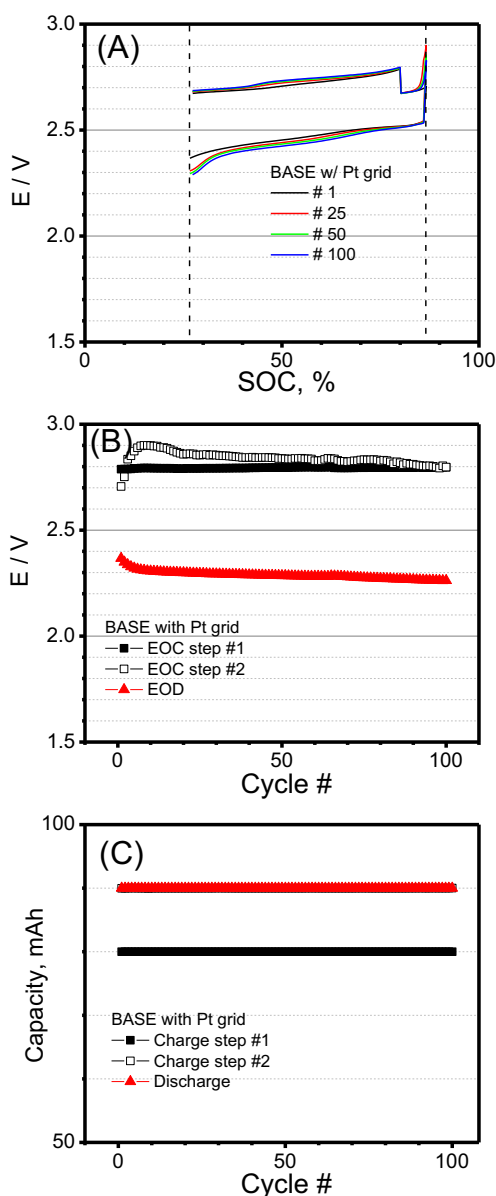


Fig. 3. Cycling performance of the cell with a metallized BASE tested under standard fixed-capacity cycling (90 mAh). (A) Voltage profiles vs. SOC, (B) EOC and EOD voltages vs. cycles, and (C) capacity vs. cycles.
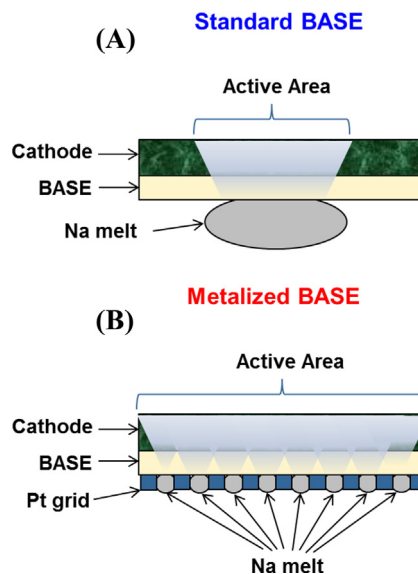


Fig. 4. Schematics of sodium distribution on the anode side of (A) a standard BASE and (B) a metallized BASE.

distribution of sodium melt on the anode side throughout the charge and discharge processes.

## 4. Conclusions

A Pt grid was applied to the BASE surface to overcome the low wettability of sodium melt on the BASE at 175 °C. These Pt-modified cells provided deeper charging than the cells with standard BASEs, and cell cycling performances were stable, unlike the standard cells. This improved performance is attributed to the better distribution of sodium melt on the BASEs and expanded active area, since molten sodium can be generated on a greater area during charging due to the electrical path provided by the Pt grid.

## Acknowledgments

## References

[1] B. Dunn, H. Kamath, J.M. Tarascon, Science 334 (2011) 928.
[2] Z.G. Yang, J.L. Zhang, M.C.W. Kintner-Meyer, X.C. Lu, D.W. Choi, J.P. Lemmon, J. Liu, Chem. Rev. 111 (2011) 3577.
[3] J.L. Sudworth, J. Power Sources 51 (1994) 105.
[4] J.L. Sudworth, R.C. Galloway, D.S. Demott, J. Electrochem. Soc. 134 (1987) C457.
[5] B.V. Ratnakumar, A.I. Attia, G. Halpert, J. Power Sources 36 (1991) 385.
[6] X.C. Lu, G.L. Li, J.Y. Kim, J.P. Lemmon, V. Sprenkle, Z.G. Yang, J. Power Sources 215 (2012) 288.
[7] G.S. Li, X.C. Lu, C.A. Coyle, J.Y. Kim, J.P. Lemmon, V.L. Sprenkle, Z.G. Yang, J. Power Sources 220 (2012) 193.
[8] J.L. Sudworth, J. Power Sources 100 (2001) 149.
[9] J.L. Sudworth, A.R. Tilley, The Sodium Sulfur Battery, Kluwer, New York, 1985.
[10] M.L. Wright, UK Pat. 2,067,005, vol. 2, 067, 005.
[11] A.V. Virkar, J.-F. Jue and K.-Z. Fung, U.S. Pat. 6,117,807, vol. 6, 117,807.